

Reduced thermal conductivity of epitaxial GaAsSb on InP due to lattice mismatch induced biaxial strain

Cite as: J. Appl. Phys. **130**, 015106 (2021); <https://doi.org/10.1063/5.0049136>

Submitted: 01 March 2021 • Accepted: 05 June 2021 • Published Online: 06 July 2021

Yuan Yuan Chu, Yuxiang Sang, Yizhe Liu, et al.



View Online



Export Citation



CrossMark

ARTICLES YOU MAY BE INTERESTED IN

Finite-temperature full random-phase approximation of bandgap narrowing in quasi-neutral regions: Theory including nonparabolicity and application to silicon and InGaAs

Journal of Applied Physics **130**, 015703 (2021); <https://doi.org/10.1063/5.0051055>

In-plane anisotropic electronic properties in layered α' -In₂Se₃

Journal of Applied Physics **130**, 015103 (2021); <https://doi.org/10.1063/5.0050979>

Normally-off operations in partially-gate-recessed AlTiO/AlGaIn/GaN field-effect transistors based on interface charge engineering

Journal of Applied Physics **130**, 014503 (2021); <https://doi.org/10.1063/5.0054045>



Webinar
Quantum Material Characterization
for Streamlined Qubit Development



Register now

Reduced thermal conductivity of epitaxial GaAsSb on InP due to lattice mismatch induced biaxial strain

Cite as: J. Appl. Phys. **130**, 015106 (2021); doi: [10.1063/5.0049136](https://doi.org/10.1063/5.0049136)

Submitted: 1 March 2021 · Accepted: 5 June 2021 ·

Published Online: 6 July 2021



View Online



Export Citation



CrossMark

Yuanyuan Chu,^{1,2} Yuxiang Sang,^{1,2} Yizhe Liu,³ Yingmei Liu,^{1,2} Zhicheng Xu,⁴ Jianxin Chen,⁴ Fang Liu,¹ Shengjuan Li,¹ Bo Sun,³ and Xingjun Wang^{2,a)}

AFFILIATIONS

¹School of Materials Science and Engineering, University of Shanghai for Science and Technology, Shanghai 200093, China

²State Key Laboratory of Infrared Physics, Shanghai Institute of Technical Physics, Chinese Academy of Sciences, Shanghai 200083, China

³Tsinghua-Berkeley Shenzhen Institute and Tsinghua Shenzhen International Graduate School, Guangdong Provincial Key Laboratory of Thermal Management Engineering and Materials, Tsinghua University, 518055 Shenzhen, Guangdong, China

⁴Key Laboratory of Infrared Imaging Materials and Detectors, Shanghai Institute of Technical Physics, Chinese Academy of Sciences, Shanghai 200083, China

^{a)}Author to whom correspondence should be addressed: xjwang@mail.sitp.ac.cn

ABSTRACT

High-quality lattice-matched and mismatched strained GaAs_{1-x}Sb_x (0.37 < x < 0.57) sub-micrometer epilayers are grown on InP by molecular beam epitaxy. Based on a heat conduction model regarding the heat transfer process between the thin GaAsSb films and thick InP substrates, the corresponding thermal conductivity of GaAsSb epilayers was accurately extracted from the power and temperature micro-Raman measurement. Combined with time-domain thermoreflectance measurements, we found that in comparison to the lattice-matched sample with Sb = 47.7%, a significant reduction in thermal conductivity of the lattice-mismatched sample with Sb = 37.9% and Sb = 56.2% is observed. With the help of diffraction reciprocal space maps and temperature-dependent photoluminescence results, the reduction in thermal conductivity is attributed to lattice-mismatch-induced biaxial tensile and compressive strain that can cause the breakage of the cubic crystal symmetry and provoke more defects.

Published under an exclusive license by AIP Publishing. <https://doi.org/10.1063/5.0049136>

I. INTRODUCTION

Alloy semiconductor GaAsSb with a tunable bandgap ranging from $\sim 0.87 \mu\text{m}$ (GaAs) to $\sim 1.7 \mu\text{m}$ (GaSb)¹⁻⁴ is suitable for a variety of potential optoelectronic applications such as optical fiber communications,³ near-infrared detectors,⁵ electron spin devices,^{6,7} quantum cascade lasers (QCLs),⁸ etc. Moreover, due to the unique band alignment, GaAsSb/InP heterostructure is more favorable for the high-speed operations double heterojunction bipolar transistor (DHBT) application.⁹ With the development of high speed, low power consumption, and high integration of micro-/nano-optoelectronics devices, efficient heat dissipation becomes particularly desirable.¹⁰⁻¹³ Knowledge of the thermal conductivity of semiconductors would provide useful guidance to the design of power dissipating devices.

Adachi has proposed a phenomenological model regarding the alloy disorder phonon scattering to calculate the thermal conductivity of semiconductor GaAsSb alloys.¹⁴ His calculation found that the thermal conductivity of GaAs_{1-x}Sb_x varied with Sb composition and reached the minimum value of $\sim 3.8 \text{ W m}^{-1} \text{ K}^{-1}$ at $x \sim 0.5$.¹⁴ However, this model does not consider the effect of strain on the thermal conductivity. The effect of strain on the thermal conductivity of solids has been widely investigated before.^{15,16} The first-principles calculation results indicate that isotropic tensile stress reduces the thermal conductivity of solids due to the reduction in both phonon group velocities and phonon lifetimes.¹⁶

There are also a lot of theoretical works focused on the effect of biaxial strain on the thermal conductivity of the

semiconductor. For example, using the first-principles calculation method, Tang *et al.*¹⁷ found that the thermal conductivity of GaN decreases under the tensile strain and increases under the compressive strain due to the changes of phonon relaxation time. Using equilibrium molecular-dynamics simulation, Li *et al.*¹⁵ thought that the thermal conductivity of silicon thin films decreases continuously when the applied strain is changed from biaxial compressive to biaxial tensile, which originated from the shift of phonon-dispersion curves under strains. Recently, using the laser-induced transient thermal grating (TTG) method, Vega-Flick *et al.*¹⁸ observed that under the biaxial tensile strain of $\sim 0.15\%$, the thermal conductivity of GaAs can be reduced by $\sim 21\%$ due to the breakage of the cubic crystal symmetry. Unfortunately, they did not discuss the effect of biaxial compressive strain on the thermal conductivity of GaAs.

Moreover, the phonon scattering can be enhanced arising from defects provoked by the lattice-mismatch-induced strain, giving rise to lowered thermal conductivity.^{19–21} Very recently, Liu *et al.* observed an abnormal S-shape behavior (blue-red-shift) that occurred in the power-dependent photoluminescence (PL) from lattice-mismatch GaAsSb/InP samples, and they attributed that to the enhanced laser heating effect caused by the lower thermal conductivity.²² However, so far, there are quite a few direct experimental evaluations of biaxial strain on the thermal conductivity of realistic III–V materials, especially for the GaAsSb film grown on InP.

The measurement of the thermal conductivity of thin films is a challenge because the heat flow cannot be directly measured. As a powerful, *in situ*, and non-contact method, the micro-Raman technique has been developed to investigate the thermal conductivity in micro-/nanoscale material systems.^{23–26} Here, the Raman laser acts as both a heat source and a thermometer simultaneously and the thermal conductivity can be determined directly.²⁶ This technique is non-destructive and not limited by the geometry and size of the sample.²⁷ More importantly, this technique may be the only choice without any nanofabrication. For example, the non-contact, time-domain thermoreflectance (TDTR)²⁸ is one of the most commonly used methods for the thermophysical properties of thin-film grown on the substrate. However, this measurement always requires coating a metal layer on the sample, which inevitably leads to contamination or damage of the sample to a certain degree. Accordingly, investigating how to extract the thermal conductivity of thin films grown on a substrate by using Raman thermometry is significant.

In this work, lattice-match and lattice-mismatch-induced strained GaAs_{1-x}Sb_x epilayers are grown on InP by molecular beam epitaxy. Through a heat conduction model taking into account the heat transfer process between thin films and thick substrates, the thermal conductivity of GaAs_{1-x}Sb_x films was extracted by power and temperature-dependent micro-Raman measurement. The thermal conductivities achieved by the Raman optothermal method were corroborated with TDTR measurements. The biaxial strain introduced by lattice-mismatch was evaluated by the XRD reciprocal space mapping. Combining with the temperature-dependent photoluminescence results, the effects of biaxial strain and induced defects on the thermal conductivity of GaAs_{1-x}Sb_x films were discussed in detail.

II. MATERIALS AND METHODS

The GaAsSb epilayers ($\sim 0.5\ \mu\text{m}$) were grown on semi-insulating InP (001) at a substrate temperature of 480 °C by molecular beam epitaxy. The Sb composition and the thickness of epilayers were determined by the XRD measurement and the scanning electron microscope, respectively.²² The optical properties were assessed by photo-luminescence (PL) using a 785 nm laser diode as the excitation source. The PL signals were dispersed by a 0.5 m grating monochromator and detected by a TE-cooled InGaAs detector. Micro-Raman scattering experiments were performed in a quasi-backscattering geometry with a 100 \times microscope lens. The Raman signals excited by a 660 nm Cobalt laser were collected by Princeton tri-vista Raman spectroscopy equipped with a liquid nitrogen-cooled Si-CCD camera. The laser power can be adjusted by using neutral density filters. For temperature-dependent Raman measurements, a hot stage was used to heat the sample. For the temperature-dependent PL spectrum measurements, the samples were mounted in a closed cycle system (Janis) with temperatures varying from ~ 6 to ~ 300 K.

A thin Al layer (~ 80 nm) was deposited onto the three samples using electron-beam evaporation for time-domain thermoreflectance (TDTR) measurements, which is a pump–probe optical technique that can be used for measuring the thermal properties of materials.²⁹ The implementation of this technique and the application of this method in investigations of the thermal conductivity of thin films can be found in our previous literature.^{28,30,31} The pump and the probe laser power were maintained at 10 and 5 mW, respectively. The surface temperature of the sample is monitored by the probe beam via the change of reflectance with temperature. The thermal conductivity of the GaAsSb film is extracted by fitting a model to the measured signal, where the magnitude and the phase depend on the thermal properties of each layer.

III. RESULTS AND DISCUSSION

Figures 1(a)–1(c) represent the asymmetric diffraction reciprocal space maps (RSMs) of samples S1 (Sb 37.9%), S2 (Sb 47.7%), and S3 (Sb 56.2%). The diffracted intensities are measured around the asymmetric (115) reciprocal lattice point of the InP substrate. The vertical dashed line denotes the location where the reciprocal lattice points of a pseudomorphic epilayer occurred. It clearly shows that the GaAsSb epilayers are grown coherently on the InP substrate, reflecting that all GaAsSb epilayers are fully strained on the InP substrates. The out-of-plane separation of the spots between the InP substrate and the GaAsSb epilayers can be converted to real space to determine Sb compositions, and biaxial strain is introduced by lattice mismatch between the epilayers and the substrate. Samples S1 and S3 are subjected to high biaxial tension of $\sim 0.43\%$ and compressive strain of $\sim -0.35\%$, respectively, whereas for lattice-matched sample S2, the corresponding biaxial strain is only $\sim 0.05\%$. Figure 1(d) is the high resolution of transmission electron microscopy (TEM) image that exhibited excellent crystalline quality and high quality of interfaces for the S3 sample.

To compare the magnitude of thermal conductivity of the lattice-matched S2 sample and the lattice-mismatched S1 (S3) sample

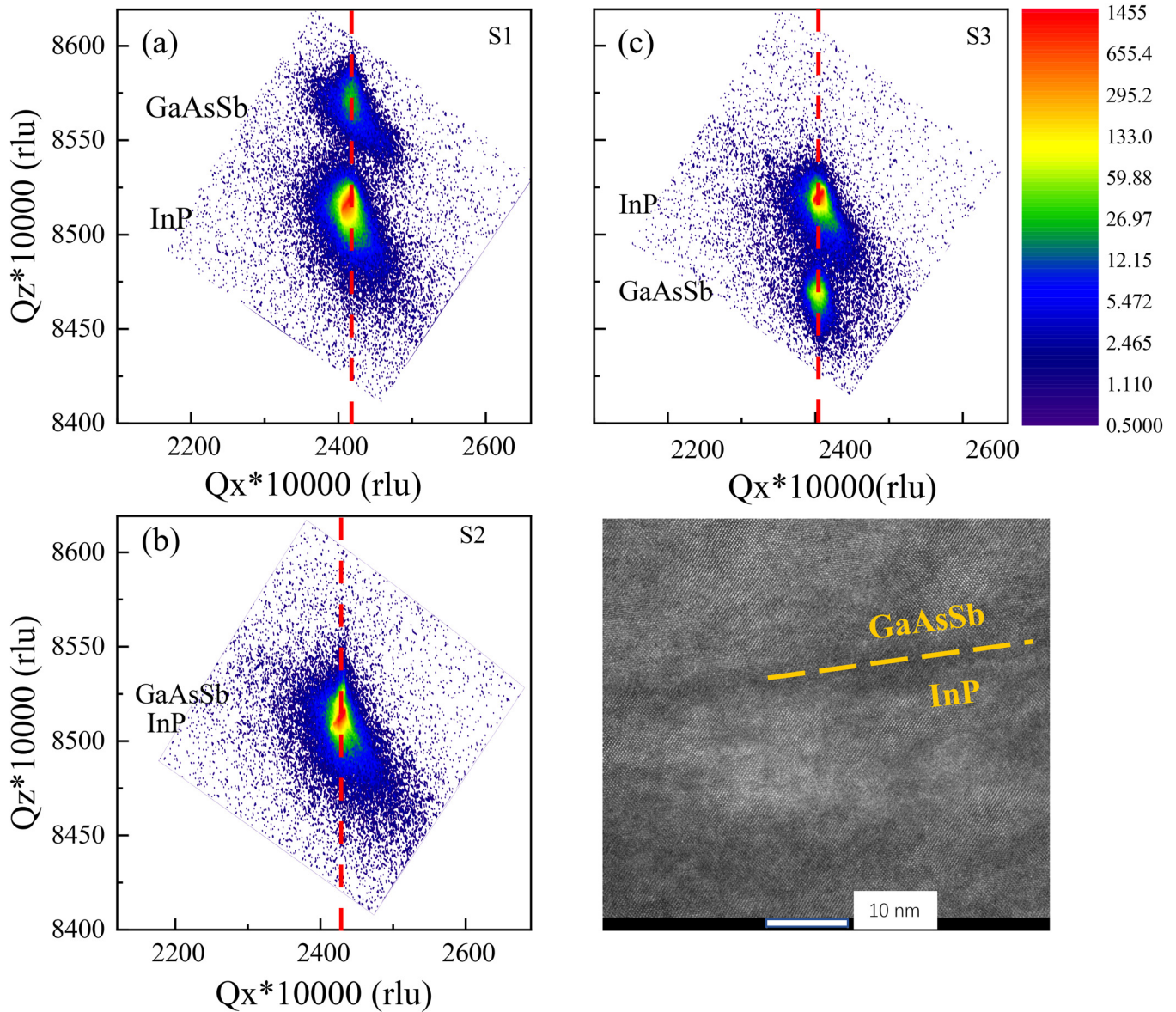


FIG. 1. (a)–(c) Asymmetrical reciprocal space mapping for the (115) reflections of the GaAsSb/InP hetero-structure with Sb ~ 37.9%, Sb ~ 47.7%, and Sb ~ 56.2%, respectively. (d) The cross-sectional TEM image of lattice-mismatched sample S3.

quantitatively, Raman measurements are employed. Assuming an approximately isothermal surface condition and the laser beam with a radial Gaussian power density, the surface temperature $T(z=0)$ for a laser spot of radius a can be derived using³²

$$\frac{\partial T}{\partial z} = f(r) = \frac{-Q}{2\pi a \kappa_a (a^2 - r^2)^{1/2}}, \quad r > 0, \quad z = 0, \quad (1)$$

where

$$T = \frac{Q}{4a \kappa_a}, \quad \kappa_a = \frac{Q}{4aT}. \quad (2)$$

For a laser beam with Gaussian distribution and beam waist given as ω , the total heat flux Q contained within radius r on the

surface can be calculated as

$$Q = P(1 - e^{-2r^2/\omega^2}). \quad (3)$$

The thermal conductivity can be written as following where the laser spot radius equals beam waist:³²

$$\kappa_a = \frac{P(1 - e^{-2})}{4aT}. \quad (4)$$

In practice, to improve measurement accuracy, a set of measurements with various excitation laser powers and temperatures were carried out and Eq. (4) can be rewritten as

$$\kappa_a = \frac{(1 - e^{-2}) \frac{\partial \Delta k}{\partial T}}{4a \frac{\partial \Delta k}{\partial P}}, \quad (5)$$

where κ_a is the thermal conductivity, P is the absorbed laser power, a is the laser spot of radius, and $\frac{\partial \Delta k}{\partial T}$ and $\frac{\partial \Delta k}{\partial P}$ are the temperature and laser power dependence of the Raman peak position, respectively. Using the measurement of P , a , $\frac{\partial \Delta k}{\partial T}$, and $\frac{\partial \Delta k}{\partial P}$, thermal conductivity κ_a can be evaluated according to Eq. (5).

Jaramillo-Fernandez *et al.*³³ investigated the effects of light penetration depth on the accuracy of the thermal conductivity by comparing the results of the finite element method (FEM) with the usual analytical approximation equation (5). They found that the

ratio between light penetration depths to laser spot radius should be smaller than 0.5 to obtain measurement errors below 10% when using the assumption of strong absorption at the surface in Eq. (5). To validate the effectiveness of Eq. (5), we first measured the laser beam spot radius with a CCD camera. The white points in Fig. 2(b) are laser beam spot size data under a focused 100× objective lens taken from the CCD camera images. The red curves are fits to the Gaussians and the laser beam radius a on the sample is determined as $\sim 0.8 \mu\text{m}$ for both x and y directions, respectively. The laser spot size could be changed by the focusing distance. Under the defocused condition, the laser beam radius on the sample is determined as $\sim 3.9 \mu\text{m}$. In our Raman setup, the laser is strongly absorbed by the sample, and the effective penetration depth (δ) can be roughly evaluated by $\delta = \frac{\lambda}{8\pi k}$, where λ is the wavelength of the incident laser and k is the extinction coefficient. For the laser with a wavelength of $\sim 660 \text{ nm}$, the value of k is about 0.374. Then, the effective penetration depth for GaAsSb was estimated to be $\sim 70 \text{ nm}$, whereas the laser spot radius was $\sim 3.9 \mu\text{m}$ and the ratio between light penetration depths to laser spot radius is only ~ 0.018 , which is much smaller than 0.5, indicating that Eq. (5) is a good approximation for calculating the thermal conductivity of a sample by which the laser is strongly absorbed.

Moreover, we crosschecked the thermal conductivity of silicon. The power and temperature-dependent Raman spectra of silicon substrate were carried out (Fig. A1 in the [supplementary material](#)). $\frac{\partial \Delta k}{\partial T}$ is estimated as $-0.021 \text{ cm}^{-1}/\text{K}$, and $\frac{\partial \Delta k}{\partial P}$ is deduced as $-0.035 \text{ cm}^{-1}/\text{mW}$ (focused condition) and $-0.009 \text{ cm}^{-1}/\text{mW}$ (defocused condition). The calculated thermal conductivity of

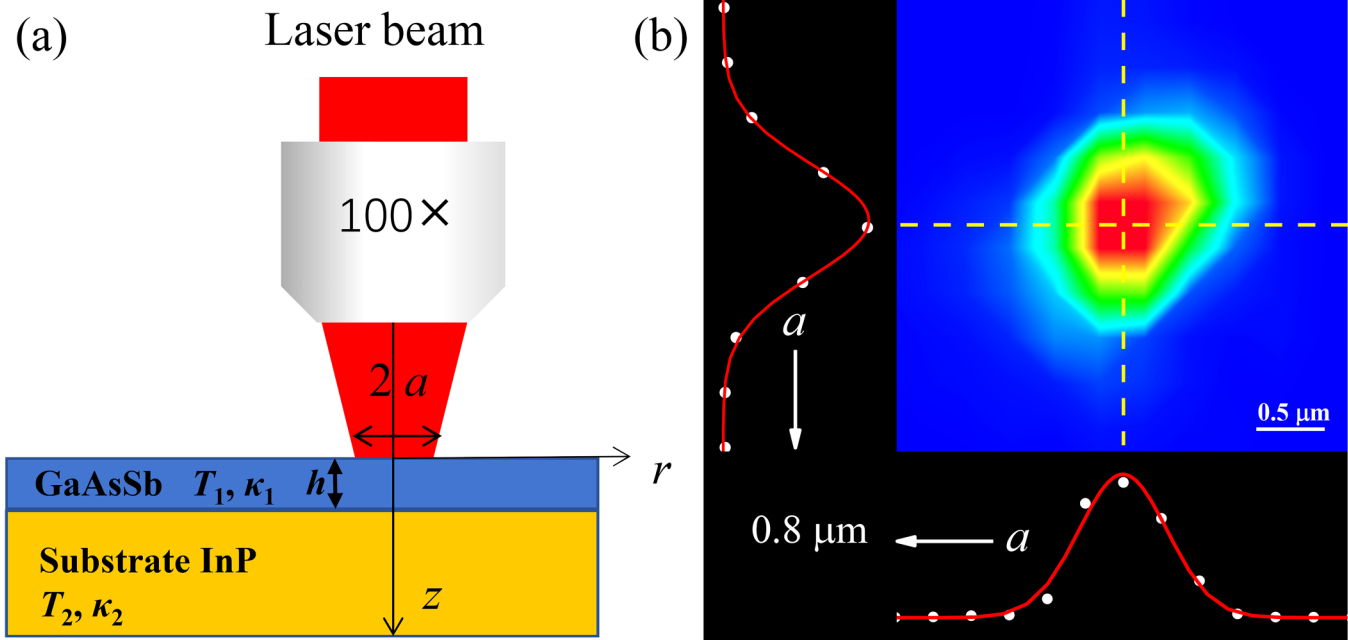


FIG. 2. (a) The schematic of the heat conduction model for GaAsSb films grown on substrate InP and (b) the spatial energy distribution of the laser beam and spot measured with a CCD under 100× objective lens. White points are laser beam spot size data and red lines are the Gaussian fitting curve of the focused spot.

silicon through Eq. (5) is $\sim 158 \text{ W m}^{-1} \text{ K}^{-1}$, which is very close to the reported thermal conductivity of silicon ($\sim 156 \text{ W m}^{-1} \text{ K}^{-1}$).³⁴

However, in the case of the GaAsSb/InP heterostructure that consists of a thick substrate (InP) and a sub-micrometer scale film (GaAsSb), the heat created by the laser beam is not only limited within the epilayer but part of the heat can also be transferred into the substrate, resulting in that the obtained thermal conductivity is just the apparent thermal conductivity of the GaAsSb/InP heterostructure rather than the thermal conductivity of GaAsSb.³⁵ To solve that, the heat transfer process between the thin films and thick substrates has to be considered. The schematic of the heat conduction model for GaAsSb/InP is drawn in Fig. 2(a). Regarding that the film thickness is much smaller than the substrate thickness, the heat conduction equations must be satisfied in both the sample and the substrate as follows:^{32,36}

$$\frac{\partial^2 T_1}{\partial r^2} + \frac{1}{r} \frac{\partial T_1}{\partial r} + \frac{\partial^2 T_1}{\partial z^2} = 0, \quad r > 0, \quad 0 < z < h, \quad (6)$$

$$\frac{\partial^2 T_2}{\partial r^2} + \frac{1}{r} \frac{\partial T_2}{\partial r} + \frac{\partial^2 T_2}{\partial z^2} = 0, \quad r > 0, \quad z > h, \quad (7)$$

where T_1 (T_2) is the temperature in the film (substrate). Continuity of the heat flow (temperature) at the interface and the boundary conditions is as follows:

$$T_1(r, z) = T_2(r, z), \quad r > 0, \quad z = h, \quad (8)$$

$$k_1 \frac{\partial T_1(r, z)}{\partial r} = k_2 \frac{\partial T_2(r, z)}{\partial r}, \quad r > 0, \quad z = h, \quad (9)$$

$$\frac{\partial T_1(r, z)}{\partial z} = -\frac{Q}{2\pi a k (a^2 - r^2)^{1/2}}, \quad a \geq r > 0, \quad z = 0, \quad (10)$$

$$\frac{\partial T_1(r, z)}{\partial z} = 0, \quad r \geq 0, \quad z = 0, \quad (11)$$

$$T_1 \text{ and } T_2 \rightarrow 0, \quad (r^2 + z^2)^{1/2} \rightarrow \infty, \quad (12)$$

where k_1 and k_2 are film and substrate thermal conductivities, respectively, and h is the film thickness. Following the theoretical work by Negus *et al.*³⁶ and Wight *et al.*,³² such isothermal contact boundary conditions are satisfied by the thermal restriction parameter listed below:

$$\frac{k_1}{4k_a} = \frac{1}{4} + \frac{2}{\pi} \sum_{n=1}^{\infty} (-1)^n \alpha^n I, \quad (13)$$

where

$$I = -2n \frac{h}{a} + \frac{1}{2} \sin^{-1}(\tau^{-1}) + (1 - \tau^{-2})^{\frac{1}{2}} \left(\tau - \frac{1}{2\tau} \right), \quad (14)$$

$$\tau = n \frac{h}{a} + \left[n^2 \left(\frac{h}{a} \right)^2 + 1 \right]^{\frac{1}{2}}, \quad (15)$$

$$\alpha = \frac{k_2 - k_1}{k_2 + k_1}. \quad (16)$$

Based on the above equations, the thermal conductivity κ_1 of the thin film can be extracted given that the laser radius a , thickness h , the apparent thermal conductivity κ_a , and the substrate thermal conductivity κ_2 are known.

Figures 3(a)–3(c) give the power-dependent Raman curves of GaAsSb. The Raman spectra are dominated by GaAs-like LO (LO_1) modes ($\sim 270 \text{ cm}^{-1}$),³⁷ which have a redshift with raising laser power from 12 to 30 mW. The redshifts are due to an anharmonic effect as a result of local laser heating on the sample. The shifts of the Raman LO modes with increasing laser power for all three samples are evident in Fig. 3(d), displaying a good linear relationship between them. It shows that the values of the slope $\frac{\partial \Delta k}{\partial P}$ are $-0.036 \text{ cm}^{-1} \text{ mW}^{-1}$ (S1 sample), $-0.029 \text{ cm}^{-1} \text{ mW}^{-1}$ (S2 sample), and $-0.074 \text{ cm}^{-1} \text{ mW}^{-1}$ (S3 sample).

Figure 4(a) displays the temperature-dependent Raman spectra of the GaAsSb sample with Sb composition of 56.2%. With an increase in temperature, LO_1 modes shift to the left (redshift) linearly due to the thermal expansion effect. The Raman peak position (Δk) vs temperature (T) for all three samples is plotted in Fig. 4(b), which exhibit a good linear relationship with a fitted slope $\frac{\partial \Delta k}{\partial T} = -0.019 \text{ cm}^{-1} \text{ K}^{-1}$ (S1), $-0.021 \text{ cm}^{-1} \text{ K}^{-1}$ (S2), and $-0.023 \text{ cm}^{-1} \text{ K}^{-1}$ (S3), respectively. It is noted that with the increase in Sb components, the slope $\frac{\partial \Delta k}{\partial T}$ slightly increases. Accordingly, $\frac{\partial \Delta k}{\partial T}$ and $\frac{\partial \Delta k}{\partial P}$ of samples S1 (Sb 37.9%), S2 (Sb 47.7%), and S3 (Sb 56.2%) have been achieved. The apparent thermal conductivity (κ_a) of the GaAsSb/InP heterostructure is, in turn, deduced as $20 \text{ W m}^{-1} \text{ K}^{-1}$ (S1), $29 \text{ W m}^{-1} \text{ K}^{-1}$ (S2), and $11 \text{ W m}^{-1} \text{ K}^{-1}$ (S3) by using Eq. (5). Furthermore, the thickness of GaAsSb epilayers is determined as $\sim 495 \text{ nm}$ (S1), 477 nm (S2), and 503 nm (S3), respectively (Fig. A2 in the [supplementary material](#)). Assuming that the thermal conductivity of the substrate InP is $\sim 68 \text{ W m}^{-1} \text{ K}^{-1}$,¹⁴ the actual thermal conductivity of the GaAsSb epilayer can be calculated according to Eq. (13), and the results are listed in Fig. 5. To verify our results, a more reliable TDTR measurement was conducted to obtain the thermal conductivity of GaAsSb, and the corresponding results are also displayed in Fig. 5.

It is noted that the interfacial thermal resistance R_K between GaAsSb and InP is not taken into account in our calculation. The reported interfacial thermal resistance R_K of InGaAs grown on InP is $\sim 10^{-10} \text{ m}^2 \text{ K/W}$.³⁸ Considering that both InGaAs and GaAsSb are III–V group alloy semiconductors owing to similar thermal conductivity, the interfacial thermal resistance R_K of GaAsSb/InP can be assumed as $\sim 10^{-10} \text{ m}^2 \text{ K/W}$. We calculated the temperature fields $T(z)$ and $T(r)$ for 500 nm thick GaAsSb grown on InP considering the interfacial thermal resistance R_K , (see Fig. A3 in the [supplementary material](#)) and found that the influence of R_K on the temperature field is negligible for $R_K \leq 10^{-8} \text{ m}^2 \text{ K/W}$.

As can be seen from Fig. 5, two sets of measured values are pretty close and the trend is similar. The thermal conductivity of

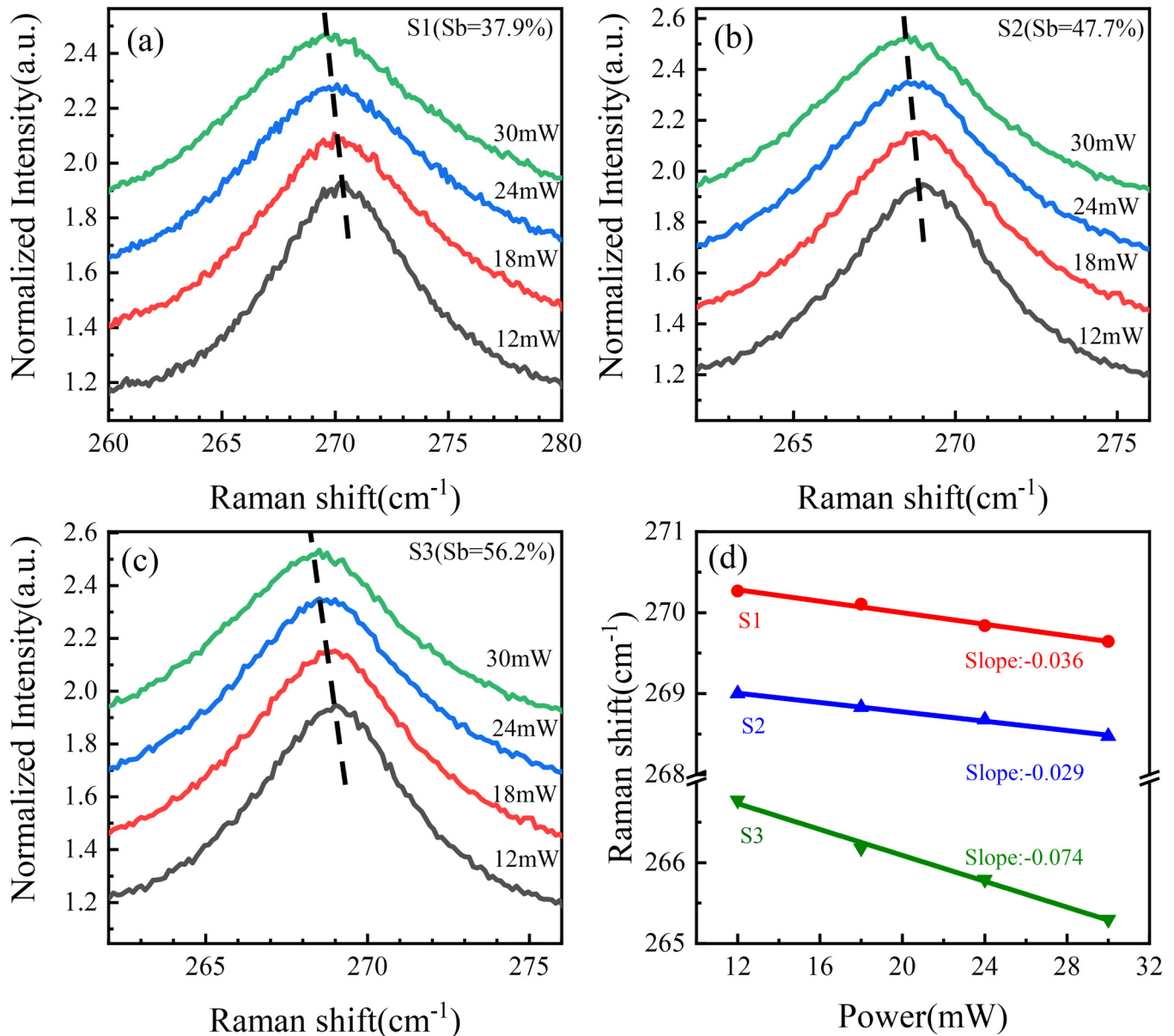


FIG. 3. (a)–(c) Power-dependent Raman spectra of GaAsSb/InP. (d) Solid lines are a linear fit for Raman peak position as a function of laser power.

GaAsSb reduced significantly compared with that of GaAs and GaSb due to alloy phonon scattering. According to the Adachi model,¹⁴ the thermal conductivity of GaAsSb is essentially unchanged between 40% and 60% of Sb. Contrastingly, in comparison to the lattice-matched sample S2 with Sb = 47.7%, we find a strong reduction rather than a little increase predicted by theory for the thermal conductivity of the lattice-mismatched sample with Sb = 37.9% and Sb = 56.2% (see the inset in Fig. 5). The discrepancy between our experiments and the theoretical curve is that Adachi's

model does not take into account the effect of strain on the thermal conductivity of GaAsSb.

In the case of GaAsSb/InP heterostructures, the in-plane biaxial strain in GaAsSb arising from the lattice mismatch would distort the cubic unit cell and break the cubic crystal symmetry with increased (decreased) lattice constants along with the interface directions and decreased (increased) lattice constant along the growth direction. Recently, Vega-Flick *et al.* found that ~0.15% in-plane biaxial tensile strain can result in ~21% reduction of the

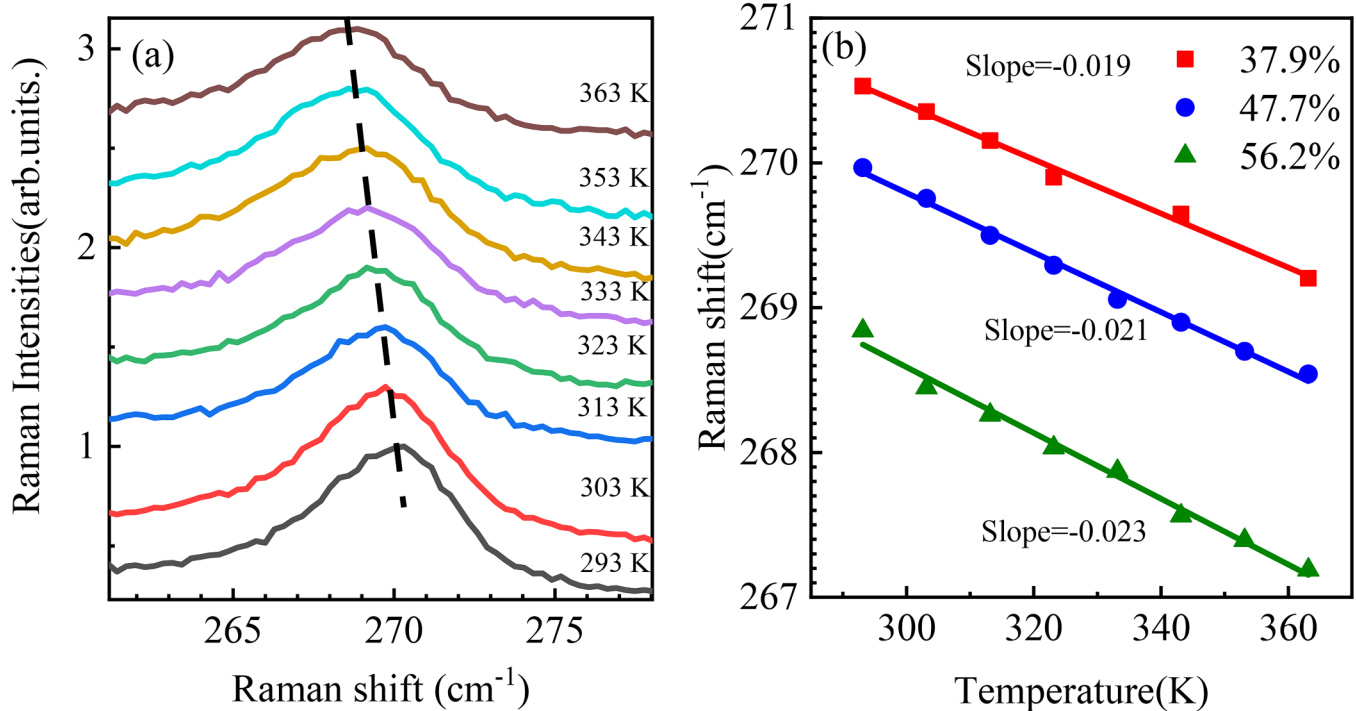


FIG. 4. (a) Temperature-dependent Raman spectra of S3 sample and (b) the measured Raman peak position vs temperature for GaAsSb/InP. The black solid lines are linear fits.

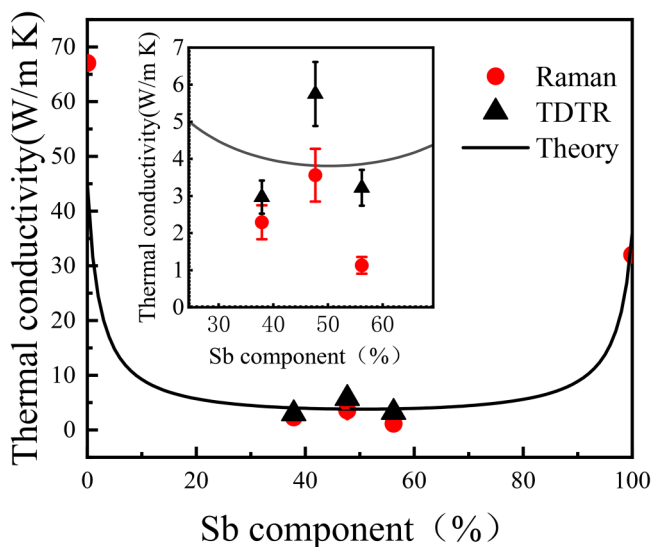


FIG. 5. Thermal conductivity vs Sb composition for $\text{GaAs}_{1-x}\text{Sb}_x$. Solid line is the calculation result of GaAsSb based on Adachi's model regarding alloy disorder scattering¹⁴ and the red solid circles represent the experimental data. The black solid triangles stand for the data measured by TDTR. The inset is the zoom-in picture.

thermal conductivity for GaAs owing to the breakage of the cubic crystal symmetry,¹⁸ which enhanced the phonon scattering rates in the stressed GaAs. As mentioned before, theoretical works pointed to an increased thermal conductivity with increasing biaxial compression strain and a decreasing thermal conductivity with increasing biaxial tensile strain. Thus, for the S1 sample with 0.43% biaxial tensile strain, the reduction in thermal conductivity is understandable. However, for the S3 sample under $\sim -0.35\%$ biaxial compressive strain, the reduction in thermal conductivity does not correspond to the theoretical prediction.

On the other hand, in the growth of lattice-mismatched epitaxial films, defects are inevitably generated.³⁹ Strain arising from hetero-epitaxial interfaces can yield increased phonon scattering due to the defects that create a mass difference at the lattice sites, leading to a strong modification of phonon scattering.²¹ Enhanced phonon scattering from defects for the lattice-mismatched sample can lead to a reduction in thermal conductivity.²⁰ Consequently, the observed overall thermal conductivity decreases under biaxial compressive strain since the effect of defect-induced reduction plays the dominant role.

To confirm that, low-temperature PL measurement was carried out to characterize the optical quality [see Fig. 6(a)]. The shift of the PL peak toward lower energies corresponds to the predicted bandgap reduction associated with an increasing Sb concentration.⁴⁰ It is noted that the lattice-matched sample S2 has the highest PL intensity and minimum FWHM (full width at half

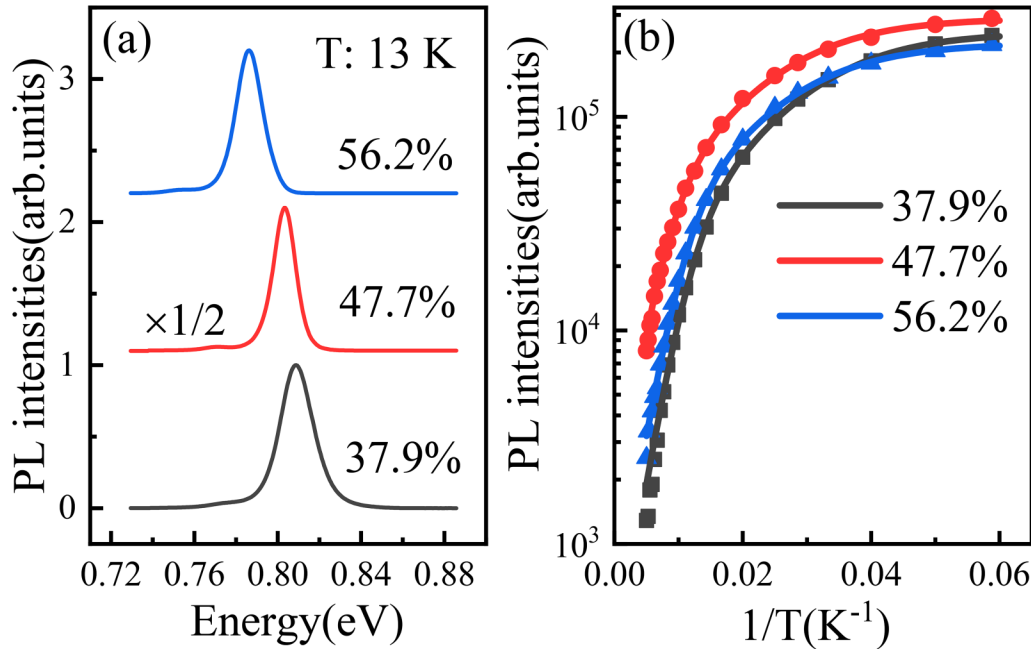


FIG. 6. (a) Low-temperature PL spectra of GaAsSb/InP heterostructure. (b) Arrhenius plot of the PL intensity measured from GaAsSb with different Sb compositions as a function of inverse temperature. The solid lines are fitting curves obtained by using Eq. (17) with parameters list in Table I.

maxima), implying lower density defects produced in sample S2. The integrated PL intensity as a function of $1/T$ for GaAsSb in the temperature range from ~ 6 to ~ 300 K is pictured in Fig. 6(b). The temperature dependence of the PL intensity can be described in terms of the Arrhenius formula, which is expressed as follows:⁴¹

$$I(T)/I(0) = 1/[1 + c_1 \exp(-E_a/KT) + c_2 \exp(-E_b/KT)], \quad (17)$$

where E_a and E_b are the thermal activation energies that are the characteristics of two thermally activated processes for high- and low- T regions, respectively, and $I(0)$ is the intensity at low T .

The corresponding activation energies E_a and E_b were found to be around ~ 8 and ~ 36 meV, respectively, as presented in Table I. The E_a channel is suggested to be correlated to the defect, and the E_b channel corresponds to the thermal-induced carrier transfer from band emission to a higher energy level.⁴² The coefficients c_1 and c_2 are proportional to the concentration of the defect centers. Compared with S1 and S3 samples, the pre-factors c_1 and

c_2 are largely reduced for the S2 sample (see Table I), demonstrating a lower defect density, which acts as a non-radiative recombination center. Such defects may enhance phonon scattering through local changes in mass, interatomic bonding forces, and strain gradients, resulting in lower thermal conductivity. Our experimental results can inspire more theoretical scientists to investigate the effect of strain on thermal conductivity taking into account both the breakage of the crystal symmetry and strain-induced defects.

IV. CONCLUSION

In this paper, we measured the power and temperature micro-Raman spectra of the lattice-matched and mismatched GaAsSb sub-micrometer epilayers grown on InP. Based on a heat conduction model considering the heat transfer process between thin films and thick substrates, the thermal conductivity of GaAsSb films was derived accurately by micro-Raman spectra. The obtained results are basically in agreement with the values measured by the TDTR method, indicating that the Raman optothermal method is an effective way to estimate the thermal conductivity of sub-micrometer films grown on substrates. Compared with the lattice-matched sample with Sb = 47.7%, we find a large reduction in thermal conductivity for the lattice-mismatched sample with Sb = 37.9% and Sb = 56.2%. Combining with the RSMs and the temperature-dependent PL results, it is suggested that biaxial tensile strain leads to a significant reduction in thermal conductivity, arising from enhanced phonon scattering that originated from the breakage of the cubic crystal symmetry and strain-induced

TABLE I. Activation energies and corresponding coefficients obtained by fitting the temperature-dependent PL intensity using Eq. (17).

GaAsSb	c_1	c_2	E_a (meV)	E_b (meV)
0.379	20	947	8	36
0.477	11	181	8	36
0.562	13	485	8	36

defects, while under biaxial compressive strain, the effect of defect-induced reduction plays the dominant role. Our results confirmed the importance of removing the stress in the epitaxial III–V alloy layers to avoid the reduction in thermal conductivity and facilitate heat dissipation.

SUPPLEMENTARY MATERIAL

See the [supplementary material](#) for power and temperature-dependent Raman spectra of silicon under focus (defocus) condition, Fourier transforms infrared (FTIR) reflection spectroscopy of GaAsSb/InP heterostructure, and the calculation of the temperature fields $T(Z)$ and $T(r)$ for 500 nm thick GaAsSb grown on InP considering different interfacial thermal resistances R_K .

ACKNOWLEDGMENTS

This work was supported by the National Natural Science Foundation of China (NNSFC) (Grant No. 11874377) and the Natural Science Foundation of Shanghai (Grant No. 18ZR1445700).

DATA AVAILABILITY

The data that support the findings of this study are available from the corresponding author upon reasonable request.

REFERENCES

- ¹E. Ahmad, M. R. Karim, S. B. Hafiz, C. L. Reynolds, Y. Liu, and S. Iyer, “A two-step growth pathway for high Sb incorporation in GaAsSb nanowires in the telecommunication wavelength range,” *Sci. Rep.* **7**, 10111 (2017).
- ²D. L. Dheeraj, G. Patriarche, L. Largeau, H. L. Zhou, A. T. van Helvoort, F. Glas, J. C. Harmand, B. O. Finland, and H. Weman, “Zinc blende GaAsSb nanowires grown by molecular beam epitaxy,” *Nanotechnology* **19**, 275605 (2008).
- ³J. Huh, D. C. Kim, A. M. Munshi, D. L. Dheeraj, D. Jang, G. T. Kim, B. O. Finland, and H. Weman, “Low frequency noise in single GaAsSb nanowires with self-induced compositional gradients,” *Nanotechnology* **27**, 385703 (2016).
- ⁴L. Ma, X. Zhang, H. Li, H. Tan, Y. Yang, Y. Xu, W. Hu, X. Zhu, X. Zhuang, and A. Pan, “Bandgap-engineered GaAsSb alloy nanowires for near-infrared photo-detection at 1.31 μm ,” *Semicond. Sci. Technol.* **30**, 105033 (2015).
- ⁵Z. Li, X. Yuan, L. Fu, K. Peng, and F. Wang, “Room temperature GaAsSb single nanowire infrared photodetectors,” *Nanotechnol.* **26**, 445202 (2015).
- ⁶W. Y. Qiu, X. J. Wang, P. P. Chen, N. Li, and W. Lu, “Optical spin polarization and Hanle effect in GaAsSb: Temperature dependence,” *Appl. Phys. Lett.* **105**, 082104 (2014).
- ⁷B. Zhang, C. Chen, J. Han, C. Jin, J. Chen, and X. Wang, “Effect of thermal annealing on carrier localization and efficiency of spin detection in GaAsSb epilayers grown on InP,” *AIP Adv.* **8**, 045021 (2018).
- ⁸H. Detz, P. Klang, A. M. Andrews, W. Schrenk, and G. Strasser, “Si doping of MBE grown bulk GaAsSb on InP,” *J. Cryst. Growth* **323**, 42 (2011).
- ⁹Y. M. Lin, C. H. Chen, J. S. Wu, and C. P. Lee, “Compositional grading in GaAsSb grown on GaAs substrates,” *J. Cryst. Growth* **402**, 151 (2014).
- ¹⁰H. Takasugi, S. Teraki, T. Kurokawa, and I. Aoki, “Development of the thin film with high thermal conductivity for power devices,” in *2014 IEEE 64th Electronic Components and Technology Conference (ECTC), Orlando, FL, 27–30 May 2014* (IEEE, 2014).
- ¹¹S. P erichon, V. Lysenko, B. Remaki, D. Barbier, and B. Champagnon, “Measurement of porous silicon thermal conductivity by micro-Raman scattering,” *J. Appl. Phys.* **86**, 4700 (1999).
- ¹²J. Anaya, S. Rossi, M. Alomari, E. Kohn, and M. Kuball, “Control of the in-plane thermal conductivity of ultra-thin nanocrystalline diamond films through the grain and grain boundary properties,” *Acta Mater.* **103**, 141 (2016).
- ¹³Y. Lin, L. Zheng, and G. Chen, “Unsteady flow and heat transfer of pseudo-plastic nanoliquid in a finite thin film on a stretching surface with variable thermal conductivity and viscous dissipation,” *Powder Technol.* **274**, 324 (2015).
- ¹⁴S. Adachi, “Lattice thermal conductivity of group-IV and III–V semiconductor alloys,” *J. Appl. Phys.* **102**, 063502 (2007).
- ¹⁵X. Li, K. Maute, M. L. Dunn, and R. Yang, “Strain effects on the thermal conductivity of nanostructures,” *Phys. Rev. B* **81**, 245318 (2010).
- ¹⁶K. D. Parrish, A. Jain, J. M. Larkin, W. A. Saidi, and A. J. H. McGaughey, “Origins of thermal conductivity changes in strained crystals,” *Phys. Rev. B* **90**, 235201 (2014).
- ¹⁷D.-S. Tang, G.-Z. Qin, M. Hu, and B.-Y. Cao, “Thermal transport properties of GaN with biaxial strain and electron-phonon coupling,” *J. Appl. Phys.* **127**, 035102 (2020).
- ¹⁸A. Vega-Flick, D. Jung, S. Yue, J. E. Bowers, and B. Liao, “Reduced thermal conductivity of epitaxial GaAs on Si due to symmetry-breaking biaxial strain,” *Phys. Rev. Mater.* **3**, 034603 (2019).
- ¹⁹J. Zou, D. Kotchetkov, A. A. Balandin, D. I. Florescu, and F. H. Pollak, “Thermal conductivity of GaN films: Effects of impurities and dislocations,” *J. Appl. Phys.* **92**, 2534 (2002).
- ²⁰K. F. Murphy, B. Piccione, M. B. Zanjani, J. R. Lukes, and D. S. Gianola, “Strain- and defect-mediated thermal conductivity in silicon nanowires,” *Nano Lett.* **14**, 3785 (2014).
- ²¹A. X. Levander, T. Tong, K. M. Yu, J. Suh, D. Fu, R. Zhang, H. Lu, W. J. Schaff, O. Dubon, W. Walukiewicz, D. G. Cahill, and J. Wu, “Effects of point defects on thermal and thermoelectric properties of InN,” *Appl. Phys. Lett.* **98**, 012108 (2011).
- ²²Y. Liu, Y. Chu, Y. Lu, Y. Li, S. Li, C. Jin, J. Chen, and X. Wang, “Lattice-optimized GaAsSb/InP heterojunction towards both efficient carrier confinement and thermal dissipation,” *Phys. Status Solidi RRL* **14**, 2000108 (2020).
- ²³Y. Yu, T. Minhaj, L. Huang, Y. Yu, and L. Cao, “In-plane and interfacial thermal conduction of two-dimensional transition-metal dichalcogenides,” *Phys. Rev. Appl.* **13**, 034059 (2020).
- ²⁴S. Xu, A. Fan, H. Wang, X. Zhang, and X. Wang, “Raman-based nanoscale thermal transport characterization: A critical review,” *Int. J. Heat Mass Transfer* **154**, 119751 (2020).
- ²⁵R. Wang, T. Wang, H. Zobeiri, P. Yuan, C. Deng, Y. Yue, S. Xu, and X. Wang, “Measurement of the thermal conductivities of suspended MoS₂ and MoSe₂ by nanosecond ET-Raman without temperature calibration and laser absorption evaluation,” *Nanoscale* **10**, 23087 (2018).
- ²⁶B. Stoib, S. Filser, N. Petermann, H. Wiggers, M. Stutzmann, and M. S. Brandt, “Thermal conductivity of mesoporous films measured by Raman spectroscopy,” *Appl. Phys. Lett.* **104**, 161907 (2014).
- ²⁷X. Liu, X. Wu, and T. Ren, “*In situ* and noncontact measurement of silicon membrane thermal conductivity,” *Appl. Phys. Lett.* **98**, 174104 (2011).
- ²⁸B. Sun and Y. K. Koh, “Understanding and eliminating artifact signals from diffusely scattered pump beam in measurements of rough samples by time-domain thermoreflectance (TDTR),” *Rev. Sci. Instrum.* **87**, 064901 (2016).
- ²⁹D. G. Cahill, “Analysis of heat flow in layered structures for time-domain thermoreflectance,” *Rev. Sci. Instrum.* **75**, 5119 (2004).
- ³⁰S. Kerdsongpanya, B. Sun, F. Eriksson, J. Jensen, J. Lu, Y. K. Koh, N. V. Nong, B. Balke, B. Alling, and P. Eklund, “Experimental and theoretical investigation of Cr_{1-x}Sc_xN solid solutions for thermoelectrics,” *J. Appl. Phys.* **120**, 215103 (2016).
- ³¹J. Ju, B. Sun, G. Haunschild, B. Loitsch, B. Stoib, M. S. Brandt, M. Stutzmann, Y. K. Koh, and G. Koblm uller, “Thermoelectric properties of In-rich InGaN and InN/InGaN superlattices,” *AIP Adv.* **6**, 045216 (2016).

- ³²N. M. Wight, E. Acosta, R. K. Vijayaraghavan, P. J. McNally, V. Smirnov, and N. S. Bennett, "A universal method for thermal conductivity measurements on micro-/nano-films with and without substrates using micro-Raman spectroscopy," *Therm. Sci. Eng. Prog.* **3**, 95 (2017).
- ³³J. Jaramillo-Fernandez, E. Chavez-Angel, and C. M. Sotomayor-Torres, "Raman thermometry analysis: Modelling assumptions revisited," *Appl. Therm. Eng.* **130**, 1175 (2018).
- ³⁴C. J. Glassbrenner and G. A. Slack, "Thermal conductivity of silicon and germanium from 3 K to the melting point," *Phys. Rev.* **134**, A1058 (1964).
- ³⁵S. Huang, X. Ruan, J. Zou, X. Fu, and H. Yang, "Thermal conductivity measurement of submicrometer-scale silicon dioxide films by an extended micro-Raman method," *Microsyst. Technol.* **15**, 837 (2009).
- ³⁶K. J. Negus, M. M. Yovanovich, and J. C. Thompson, "Constriction resistance of circular contacts on coated surfaces: Effect of boundary conditions," *J. Thermophys. Heat Transfer* **2**, 158 (1988).
- ³⁷R. Cohen, M. Cherng, R. Benner, and G. Stringfellow, "Raman and photoluminescence spectra of GaAsSb," *J. Appl. Phys.* **57**, 4817 (1985).
- ³⁸A. Sood, J. A. Rowlette, C. G. Caneau, E. Bozorg-Grayeli, M. Asheghi, and K. E. Goodson, "Thermal conduction in lattice-matched superlattices of InGaAs/InAlAs," *Appl. Phys. Lett.* **105**, 051909 (2014).
- ³⁹H.-Q. Nguyen, E. Y. Chang, H.-W. Yu, H.-D. Trinh, C.-F. Dee, Y.-Y. Wong, C.-H. Hsu, B.-T. Tran, and C.-C. Chung, "Threading dislocation blocking in metamorphic InGaAs/GaAs for growing high-quality $\text{In}_{0.5}\text{Ga}_{0.5}\text{As}$ and $\text{In}_{0.3}\text{Ga}_{0.7}\text{As}$ on GaAs substrate by using metal organic chemical vapor deposition," *Appl. Phys. Express* **5**, 055503 (2012).
- ⁴⁰R. Lukic-Zrnica, B. P. Gorman, R. J. Cottier, T. D. Golding, C. L. Littler, and A. G. Norman, "Temperature dependence of the band gap of GaAsSb epilayers," *J. Appl. Phys.* **92**, 6939 (2002).
- ⁴¹I. A. Buyanova, M. Izadifard, W. M. Chen, A. Polimeni, M. Capizzi, H. P. Xin, and C. W. Tu, "Hydrogen-induced improvements in optical quality of GaNAs alloys," *Appl. Phys. Lett.* **82**, 3662 (2003).
- ⁴²X. Chen, Q. Zhuang, H. Alradhi, Z. M. Jin, L. Zhu, X. Chen, and J. Shao, "Midinfrared photoluminescence up to 290 K reveals radiative mechanisms and substrate doping-type effects of InAs nanowires," *Nano Lett.* **17**, 1545 (2017).